2012

Observation of Sulfate Aerosols and SO_2 From the Sarychev Volcanic Eruption Using Data From the Atmospheric Chemistry Experiment (ACE)

D. Doeringer

A. Eldering

C. D. Boone

G. González Abad

P. F. Bernath
Old Dominion University, pbernath@odu.edu

Original Publication Citation

Doeringer, D., Eldering, A., Boone, C. D., González Abad, G., & Bernath, P. F. (2012). Observation of sulfate aerosols and SO_2 from the sarychev volcanic eruption using data from the atmospheric chemistry experiment (ACE). *Journal of Geophysical Research: Atmospheres, 117*(D3), 1-15, Article D03203. https://doi.org/10.1029/2011JD016556

Observation of sulfate aerosols and SO_2 from the Sarychev volcanic eruption using data from the Atmospheric Chemistry Experiment (ACE)

D. Doeringer,[1] A. Eldering,[2,3] C. D. Boone,[4] G. González Abad,[5] and P. F. Bernath[5]

Received 14 July 2011; revised 27 November 2011; accepted 30 November 2011; published 4 February 2012.

[1] Infrared spectra measured by the Atmospheric Chemistry Experiment Fourier Transform Spectrometer (ACE-FTS) on the SCISAT satellite were used to analyze the Sarychev volcanic aerosol after the eruption in June 2009. Evidence of the Sarychev eruptions was first detected in July 2009 from enhanced SO_2 concentrations and atmospheric extinction. By February 2010, the atmosphere had returned to pre-Sarychev conditions. In July 2009, the volcanic plume was found between 8.5 km and 17.5 km in altitude at mid- and high latitudes (55°N–70°N). The first SO_2 and sulfate aerosol retrievals carried out using the infrared solar occultation spectra recorded with the ACE-FTS are presented here. The size distribution parameters, the aerosol volume slant column and the composition of the sulfate aerosol were obtained by using a least squares algorithm. The maximum volume slant column of the aerosols was found to be 850 μm^3 cm^{-3} km, which results in an approximate aerosol loading of 3 μm^3 cm^{-3}. One month after the eruption, the composition of the aerosols providing the best-fit is a 75% sulfuric acid-water solution with an effective radius (R_{eff}) of 0.1–0.3 μm.

Citation: Doeringer, D., A. Eldering, C. D. Boone, G. González Abad, and P. F. Bernath (2012), Observation of sulfate aerosols and SO_2 from the Sarychev volcanic eruption using data from the Atmospheric Chemistry Experiment (ACE), *J. Geophys. Res.*, *117*, D03203, doi:10.1029/2011JD016556.

1. Introduction

[2] Large volcanic eruptions have a significant impact on the atmosphere. They affect climate by increasing the cloud albedo and reflecting more solar radiation to space, which leads to a net cooling of the lower atmosphere. Sulfuric acid aerosols and small dust particles are primarily responsible for this cooling [*Pollack et al.*, 1976]. All major volcanic eruptions in the last 50 years have increased the total optical depth in the lower stratosphere and upper troposphere [*Sato et al.*, 1993]. For example, the eruption of Mt. Pinatubo in 1991 caused a decrease in temperature of 0.7 K in the lower troposphere of the Northern Hemisphere in September 1992 [*Dutton and Christy*, 1992] and increased the atmospheric optical depth at 550 nm to approximately 0.15–0.20 [*Sato et al.*, 1993]. However, the absorption of infrared radiation by larger aerosols causes a net warming inside the plume [*Pollack et al.*, 1976]. Strato-volcanic eruptions emit aerosols and sulfur dioxide into the lower stratosphere, where sulfuric acid particles have a longer lifetime. Due to their longer lifetime, stratospheric sulfate acid particles have a stronger and more significant effect on the scattering of solar radiation than sulphate acid particles in the troposphere.

[3] The emitted sulfur dioxide molecules (SO_2) are slowly oxidized by OH radicals to form the sulfuric acid molecule (H_2SO_4), this process occurs in the troposphere as well as in the stratosphere and happens on a timescale of several weeks. The oxidation from SO_2 to H_2SO_4 takes place in three steps [*Reiner and Arnold*, 1994]:

$$SO_2 + OH + M \rightarrow HSO_3 + M \quad (1)$$

$$HSO_3 + O_2 \rightarrow SO_3 + HO_2 \quad (2)$$

$$SO_3 + H_2O + M \rightarrow H_2SO_4 + M \quad (3)$$

However, the sulfuric acid in the troposphere also originates from aqueous oxidation of SO_2 by H_2O_2 in cloud droplets [*Reeves and Penkett*, 2003]:

$$SO_2 + H_2O \rightleftharpoons H^+ + SO_2OH^- \quad (4)$$

$$SO_2OH^- + H_2O_2 \rightleftharpoons SO_2OOH^- + H_2O \quad (5)$$

$$SO_2OOH^- + H^+(HA) \rightarrow H_2SO_4 + (A^-) \quad (6)$$

[1]Department of Physics, University of York, York, UK.
[2]Jet Propulsion Laboratory, Pasadena, California, USA.
[3]Department of Atmospheric Science, University of California, Los Angeles, California, USA.
[4]Department of Chemistry, University of Waterloo, Waterloo, Ontario, Canada.
[5]Department of Chemistry, University of York, York, UK.

0148-0227/12/2011JD016556

Reactions (1)–(6) are the main oxidation pathways for the removal of SO_2 from the troposphere, it is believed that 60–80% of tropospheric SO_2 are removed by the aqueous phase process [*Reeves and Penkett*, 2003].

[4] In this paper ACE observations of the eruption of Sarychev (located at 48°N, 153°E) are presented. Sarychev erupted explosively between 12 and 17 June 2009 with a plume that rose up to altitudes of 8–16 km (AURA Cloud/Aerosol/SO_2 Working Group, Summary of volcanic activity, 2009, based upon information from Smithsonian Institution, http://www.volcano.si.edu/reports/bulletin/index.cfm) and perhaps as high as 21 km. During this period ash and approximately 1.2 ± 0.2 Tg of SO_2 were injected in the upper troposphere and lower stratosphere [*Haywood et al.*, 2010].

[5] The aim of this paper is to show the temporal and spatial variation of volcanic plumes using ACE data with Sarychev origin. From ACE observations, it is possible to obtain atmospheric extinction at 1.02 μm, SO_2 concentration profiles and sulfate aerosol loading, as well as some aerosol size parameter information in favorable occultations. A substantial aerosol layer has been found in the upper troposphere and lower stratosphere (between 8.5 km and 17.5 km) in the month of July 2009 in the Northern Hemisphere after the Sarychev eruption. The temporal variation of the atmospheric optical depth shows a significant enhancement after the Sarychev eruptions. This enhancement of the optical depth lasted 8 months, returning to pre-Sarychev eruption values in February 2010. The volcanic aerosol properties for certain occultations in July 2009 are retrieved using a χ^2-minimizing method with a unimodal lognormal size distribution model. The retrieved slant columns are inverted into an aerosol loading to estimate the vertical concentration profile. The wide spectral range (750–4400 cm^{-1}) of the ACE Fourier transform spectrometer provides some information about the aerosol size distribution and makes it possible to derive the median radius r_g of a unimodal lognormal size distribution in favorable cases.

2. ACE Satellite

[6] The Atmospheric Chemistry Experiment (ACE) mission, also known as SCISAT, of the Canadian Space Agency (CSA) was launched by the National Aeronautics and Space Administration (NASA) on 12 August 2003. The satellite covers tropical, midlatitude and polar regions due to the circular low Earth orbit (650 km) with an orbital inclination of 74° [*Bernath et al.*, 2005]. ACE is equipped with three instruments with the original main science goal of improving our understanding of polar ozone chemistry. The observation technique is solar occultation at sunrise (sr) and sunset (ss) using primarily a high-resolution infrared Fourier transform spectrometer (FTS), which covers the 750–4400 cm^{-1} spectral region with a resolution of 0.02 cm^{-1}. The FTS has a vertical resolution of about 3–4 km as set by the field-of-view from the top of the clouds to 150 km. The infrared spectra provide height profiles for a large number of atmospheric trace gases (see http://www.ace.uwaterloo.ca/) as well as the meteorological variables of temperature and pressure. The near infrared and visible spectra (400–1030 nm, with a spectral resolution of 1–2 nm) are measured with the MAESTRO (Measurement of Aerosol Extinction in the Stratosphere and TRoposphere by Occultation) instrument to obtain profiles of atmospheric extinction, nitrogen dioxide and ozone [*Bernath et al.*, 2005; *McElroy et al.*, 2007]. Two filtered imagers monitor clouds and aerosols by measuring the atmospheric extinction in the near-infrared region (NIR) at 1030 nm and in the visible region (VIS) at 525 nm. At these wavelengths the spectrum is dominated by Rayleigh, aerosol and cloud scattering with a contribution from ozone, particularly at 525 nm. The description of the retrieval algorithm for extinction can be found in *Gilbert et al.* [2007] and an evaluation of the utility of the NIR Imager is given in *Vanhellemont et al.* [2008]. Although the NIR Imager aerosol extinction product has a systematic high bias relative to other instruments, the data is useful for scientific purposes [*Vanhellemont et al.*, 2008].

3. Method

[7] In this paper the atmospheric extinction from NIR imager measurements, the SO_2 volume mixing ratios (VMRs) derived from the FTS data and aerosol properties estimated from "continuum" spectra of the ACE-FTS data are used to scrutinize the volcanic plume after the Sarychev volcanic eruption.

3.1. Sulfur Dioxide

[8] The SO_2 retrieval is a research version based on the same global-fit method with a Levenberg-Marquardt nonlinear least squares fitting algorithm used in the version 2.2 processing as described by *Boone et al.* [2005]. The pressures and the temperatures used are from ACE-FTS version 3.0 processing. The altitude range of the retrievals is between 12 km and 25 km and covers, therefore, the lower stratosphere and for lower latitudes also the upper troposphere. For the retrievals, four microwindows have been used: (1) centered at 1367.80 cm^{-1} with a width of 1.0 cm^{-1}, (2) centered at 1370.25 cm^{-1} with a width of 0.7 cm^{-1}, (3) centered at 1371.55 cm^{-1} with a width of 0.8 cm^{-1}, and (4) centered at 1376.30 cm^{-1} with a width of 0.6 cm^{-1}. The spectroscopic data for SO_2 are used from HITRAN 2004 [*Rothman et al.*, 2005]. Note that potential SO_2 microwindows at lower wave numbers were discarded in order to minimize the influence of what appears to be an HNO_3 band missing from the HITRAN line list. Interferers in these microwindows are H_2O, $H_2^{18}O$, $H_2^{17}O$, HDO, $CO^{18}O$, $CO^{17}O$, O_3, CH_4, $^{13}CH_4$, CH_3D, HCN, CH_3Cl and C_2H_2. The ACE retrieval assumes horizontal homogeneity so the retrieved concentrations are likely lower limits for the plumes. An example of an occultation spectrum (ss31868) with a clear SO_2 signature is shown in Figure 1, displaying the measured spectra, the contribution of the SO_2 to the spectrum and the fitting residuals (observed minus calculated spectral points) with and without SO_2 in the calculated spectrum. The residuals without SO_2 show the shape of the SO_2 contribution and the residuals with SO_2 included are significantly smaller and improved. Note the different vertical scales for the residuals with and without SO_2.

[9] For background SO_2 concentrations the retrieved profiles are dominated by noise, meaning that the statistical error is larger than or about the same magnitude as the derived VMR in the retrieval. As explained by *Boone et al.* [2005], the error in the retrieval results from two

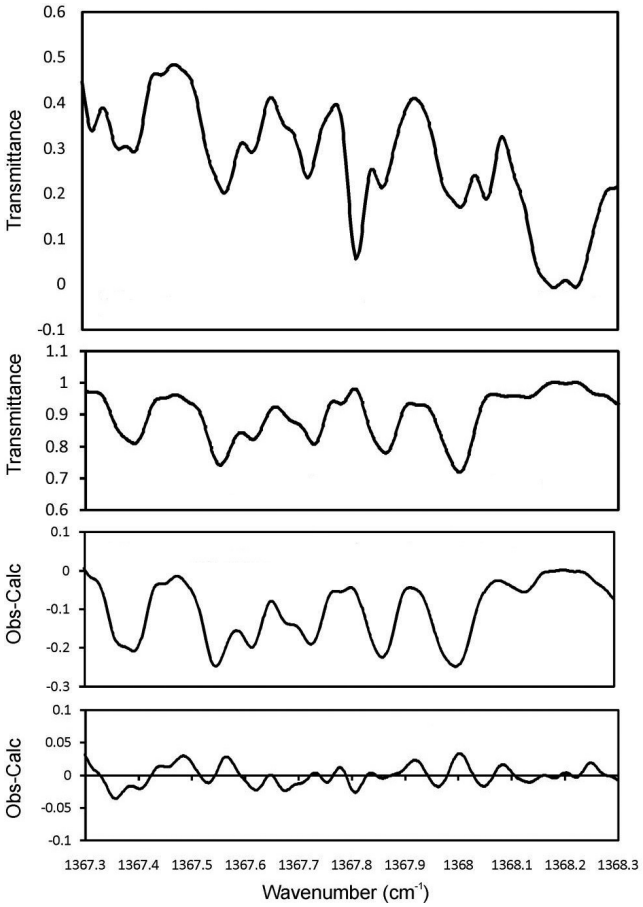

Figure 1. Illustration of an occultation spectrum (ss31868) with a clear SO_2 signature (4.6 ppb). (top to bottom) The measured spectrum at 14.8 km, the contribution of SO_2, the residuals without the contribution of SO_2 in the forward model, and the residuals with SO_2 included in the forward model.

components, the statistical fitting error or random error and the systematic error. The statistical error Δx_{stat} for the retrievals is on average about 0.01 ppb and when the VMRs are enhanced by about 0.1 ppb, the retrieval is very reliable. The systematic error in the retrieval results from the uncertainties of relevant parameters in the fitting process. The effects of the error on these parameters has been analyzed using a method similar to *González Abad et al.* [2011]:

$$\Delta x_{syst} = \sqrt{\left(\sum_j |x(b_j) - x(b_j + \Delta b_j)|^2\right)} \qquad (7)$$

The error Δx_{syst} due to the systematic error in the VMR, results from the difference of the unperturbed $x(b_j)$ and perturbed $x(b_j + \Delta b_j)$ retrieved VMR, using 1σ of its assumed uncertainty (Δb_j). The relevant parameters b_j (and their 1σ uncertainty) were considered to be the temperature (2 K), the tangent height (150 m), the instrumental line shape ILS (5% of field of view) [*Sica et al.*, 2008; *Dufour et al.*, 2009], the uncertainties in the spectroscopic data (15% for SO_2) [*Rothman et al.*, 2005], the mixing ratio of the main interferers H_2O (5%), CO_2 (1%), CH_4 (5%) and O_3 (5%) [*McHugh et al.*, 2005]. For the analysis of the systematic error of the SO_2 retrieval, 15 occultations with a clear SO_2 signature have been selected from July 2009. Figures 2a and 2b show the systematic error due to the uncertainty of different parameters and the statistical error. In Figure 2a the mean VMR of SO_2 (black) is plotted with the systematic and statistical errors. The result in Figure 2 shows a high sensitivity of the uncertainty to the tangent height, resulting in a more significant error, about 0.1 ppb at a VMR of 1 ppb, than the statistical error. The uncertainty of the other parameters does not have a significant influence on the systematic error. The relative error is shown in Figure 2b, where the error due to the uncertainty of the tangent height results in a 5%–10% error relative to the VMR of SO_2 for a height where a clear signal of SO_2 is present (between 12.5 km and 17.5 km). The statistical error for the VMR is about 0.01 ppb, approximately 1% of the VMR (between 12.5 km and 17.5 km). The systematic error has been observed also for lower SO_2 VMRs (≤0.5 ppb), resulting in a systematic error of 5%–25% of the retrieved VMR. Due to the very low atmospheric concentration above 18 km the relative errors increase sharply.

[10] Elevated concentrations of SO_2 are generally associated with volcanic plumes, so measurable sulfur dioxide concentrations are used as a verification of the existence of volcanic influence in occultations. Figure 3 shows the total number of occultations with measurable SO_2 VMRs from the beginning of 2005 to the end of 2009. Note that the fraction of occultations with enhanced SO_2 is not presented because the number of occultations and their location vary so much [*Foucher et al.*, 2011]. It is shown that ACE-FTS observes reliable, enhanced SO_2 concentrations (≥0.1 ppb, with a statistical error of about 0.01 ppb) after a major volcanic event. Accordingly, significantly enhanced sulfur dioxide is measured in 2008 after the eruption of Kasatochi (August 2008) and in 2009 after the eruption of Sarychev (July 2009), as illustrated in Figure 3. A few occultations with enhanced SO_2 can also be found in 2005, where they are likely to be from the eruptions of Anatahan (Marina Islands), Soufriere (West Indies) and Colima (western Mexico). However, there are only a few occultations with enhanced SO_2 for these eruptions due to the low global coverage by ACE and a relatively low stratospheric SO_2 injection, compared to the eruption of Kasatochi and Sarychev.

3.2. Aerosol Properties

[11] To derive aerosol properties from ACE-FTS spectra, "continuum" spectra are used. From the raw ACE-FTS spectra at each observed tangent altitude all known molecules are removed using the version 3.0 forward model (see http://ace.uwaterloo.ca/ for a list of species). Residual spectra are calculated by ratioing the observed spectra with the calculated spectra. In each residual spectrum 500 points are averaged on a fixed interpolated wave number grid (with a point spacing of 0.00125 cm^{-1}) to get a spectrum with a point spacing of 0.625 cm^{-1} and the resulting standard deviation is used as an estimate of the observational error. To exclude the regions of strong absorption, only points with a transmission greater than 0.5 were included. The points were then linearly interpolated on a 2 cm^{-1} grid to give a

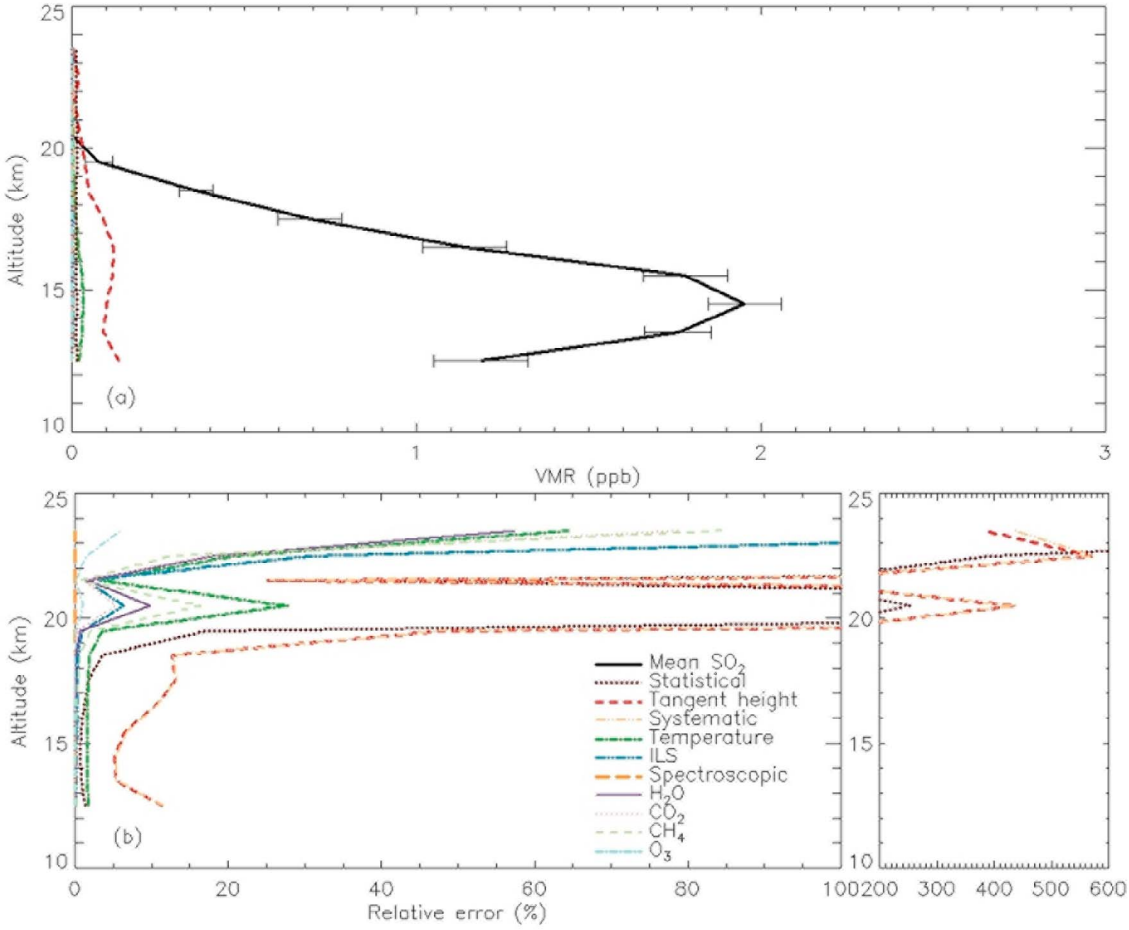

Figure 2. The mean error of 15 selected occultations in July 2009 due to the uncertainty of different parameters and the statistical error is shown. (a) The error (ppb) in comparison to the VMR of the retrieval (black line) with the corresponding total error $\Delta x = \sqrt{\Delta x_{syst}^2 + \Delta x_{stat}^2}$ (shown as error bars) and (b) the relative errors. The retrieval shows a high sensitivity to the uncertainty of the tangent height, resulting in a larger error than the statistical error. The systematic error, dominated by the uncertainty of the tangent height is about 0.1 ppv and, therefore, is between 5% and 10% of the VMR of SO_2 (between 12.5 km and 17.5 km). The uncertainty in the other parameters does not have a significant influence on the systematic error.

"measured" spectrum called K_{meas} and a standard error of the measurement ΔK_{meas}. The spectrum of the atmosphere is dominated by absorption lines of several trace gases, such as water vapor, ozone, and carbon dioxide. It is difficult to separate the broad aerosol absorption bands from sharper molecular lines and this is best accomplished using high resolution spectra. Fourier transform spectrometers (e.g., ACE [*Bernath et al.*, 2005], Atmospheric Trace Molecule Spectroscopy (ATMOS) [*Gunson et al.*, 1996]) have the required combination of high resolution, high signal-to-noise ratio and broad spectral bandwidth for the analysis method used in this paper [*Eldering et al.*, 2001, 2004; *Steele et al.*, 2003, 2006].

[12] We follow the method described by *Eldering et al.* [2001] to extract aerosol properties from the observed spectrum K_{meas} by using a forward model to compute a modeled spectrum K_{model} and adjusting the aerosol properties to minimize the residuals, $K_{meas} - K_{model}$. For the estimation of values for several of the aerosol properties, namely the volume slant column *SC* (the total volume of aerosol in the total column between the Sun and the detector in units of μm^3 of aerosol per cm^2 along the slant path in km), the weight percent *W* of sulfuric acid in the aerosol droplets, the radius r_g and the distribution width σ, which is the standard deviation of a lognormal distribution (defined below), six selected wave number ranges between 800 cm^{-1} and 4100 cm^{-1} are used. Certain wave number ranges cannot be used due to total absorption by trace gases and the presence of nitrogen, oxygen, water and carbon dioxide continua not included in the ACE forward model. The six wave number ranges employed are: (1) a range between 820 and 920 cm^{-1}, (2) 1072–1240 cm^{-1}, (3) 1850–2040 cm^{-1}, (4) between 2680 and 2880 cm^{-1}, (5) 3230–3480 cm^{-1} and (6) 3900–4050 cm^{-1}. The regions (1) and (2) contain significant H_2SO_4 absorption features and minimal interference from other trace gases [*Eldering et al.*, 2001]. In the end 571

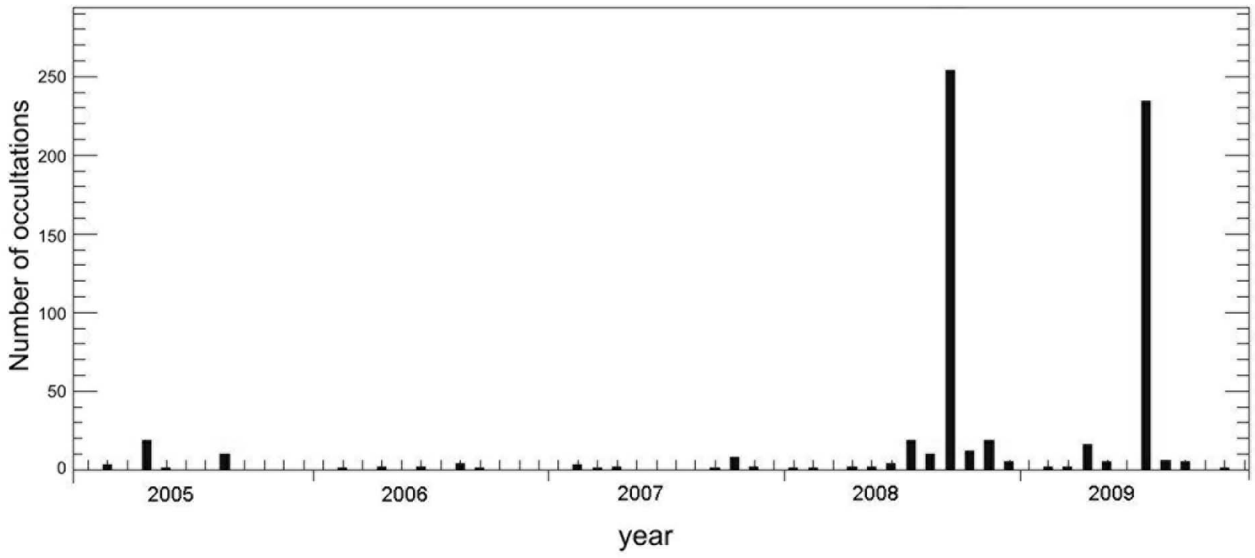

Figure 3. Number of occultations with a maximum SO_2 VMR ≥ 0.1 ppb between 2005 and 2009 from ACE-FTS data.

spectral points were chosen to retrieve the aerosol properties. Low wave numbers (region (1) and region (2)) only provide information about the aerosol volume and the composition, and it is the wide spectral range of ACE-FTS spectra makes it possible to obtain some information on the aerosol size distribution.

[13] In our analysis, we fitted three or four free parameters, including the aerosol volume slant column *SC*, the composition or weight percent *W*, an offset α and depending on the analysis the aerosol size parameter r_g using a set of 571 data points (from inside the 6 wave number ranges) from the "continuum" spectrum of an ACE occultation. The offset is useful if there are non-linearities in the detector or extinction of the radiation from a high concentration of particles, which results in changes to the overall signal level. A continuum spectrum K_{meas} is compared to a modeled aerosol spectrum K_{model} and the parameters are adjusted using a non-linear least squares fitting procedure that minimizes the residuals. An iterative algorithm has been employed to find the minimum χ^2 value, which is defined below (see equation (11)). The modeled aerosol spectrum depends on a modeled extinction spectrum β_{model} and *SC*, expressed by:

$$K_{model}(\nu) = \alpha \cdot \prod_i \exp\left(-\int_x \beta_{model,i}(\nu, x) \cdot SC_i(x) dx\right) \quad (8)$$

$$= \alpha \cdot \prod_i \exp\left(-\beta_{model,i}(\nu) \cdot SC_i\right) \quad (9)$$

with *i* representing the wide variety of aerosols that could be included and the offset α. To determine β_{model}, the Aerosol Extinction Estimation Program (AXE) [*Eldering et al.*, 2001] is used to calculate Mie extinctions between 800 and 4200 cm^{-1} in 2 cm^{-1} microwindows by using refractive index data. In our analysis the extinction of H_2SO_4 aerosols were used, as the large majority of the volcanic aerosol seems to be aqueous H_2SO_4 droplets [*Sheridan et al.*, 1992]. The refractive indices for the modeled spectra are taken from *Tisdale et al.* [1998] and a unimodal lognormal size distribution is employed [*Pinnick et al.*, 1976]:

$$\frac{dN(r)}{dr} = \frac{N_0}{r \ln\sigma \sqrt{2\pi}} \exp\left[-\frac{\ln^2(r/r_g)}{2\ln^2\sigma}\right], \quad (10)$$

where $\frac{dN(r)}{dr}$ is the concentration of particles per unit radius interval, with the total concentration of particles N_0, the median radius r_g and the distribution width σ.

[14] To determine the quality of the sulfate aerosol retrieval, the χ^2 value is calculated. This parameter indicates how well the modeled spectrum K_{model} reproduces the observed spectrum K_{meas}, and is defined as:

$$\chi^2 = \frac{1}{N} \cdot \sum_{k=1}^{N} \left[\frac{K_{meas}(\nu_k) - K_{model}(\nu_k)}{\Delta K_{meas}(\nu_k)}\right]^2, \quad (11)$$

in which *N* are the degrees of freedom, which is the difference between the number of independent points (571) and the number of free parameters (3 or 4) in the least squares fitting.

[15] Figures 4a and 4b show examples for two occultations with Sarychev volcanic aerosol signals. These spectra (ss31868 and ss31976) were measured on 14 July 2009 (68.31°N, 18.86°W) and 21 July 2009 (63.51°N, 176.37°W), respectively, and display sulfate aerosol extinction. The maximum SO_2 VMR was found to be $[SO_2] = 4.73 \pm 0.07$ ppb (ss31868) and $[SO_2] = 1.73 \pm 0.06$ ppb (ss31976). Figure 4 shows that the modeled spectrum (red) follows the shape of the observed continuum spectrum (black) quite well with a $\chi^2 \approx 2.6$ and $\chi^2 \approx 1.4$, respectively, for a fixed $\sigma = 1.8$ (see below for a justification of this choice) and floated values *SC*, *W* and r_g at a tangent height of about 15 km (height of the maximum SO_2 VMR).

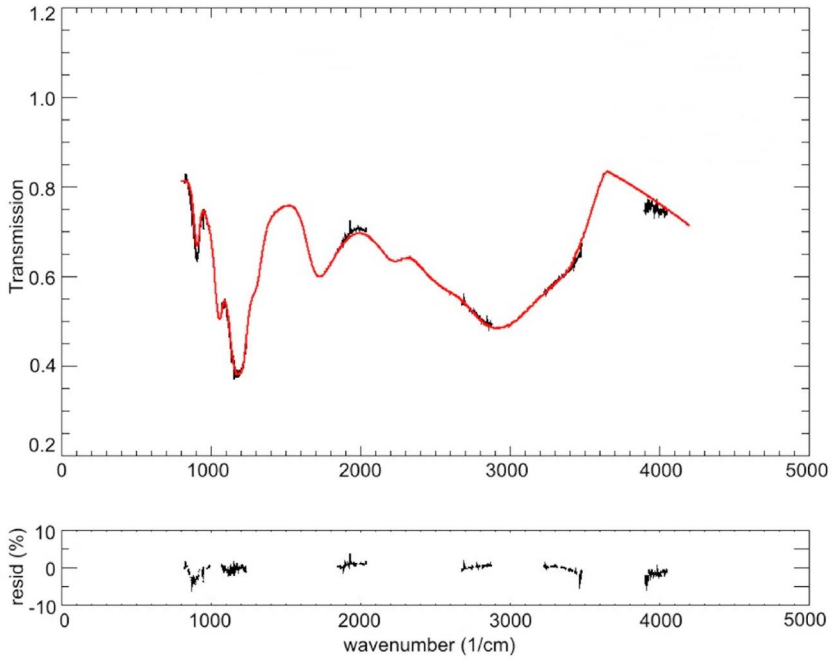

(a) ss31868 (14.07.2009, 68.31°N, 18.86°W) at 14.784 km

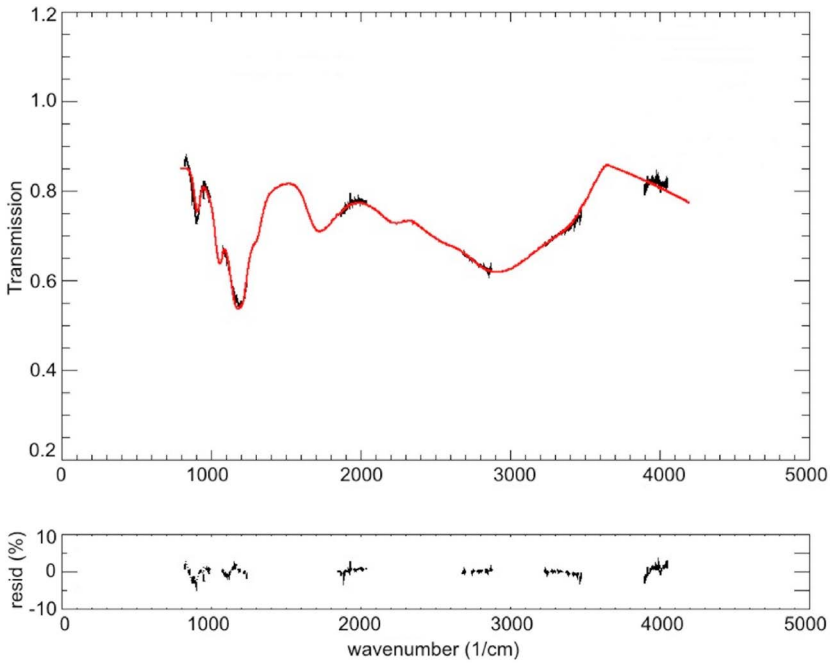

(b) ss31976 (21.07.2009, 63.51°N, 176.37°W) at 15.815 km

Figure 4. ΔK_{meas} (black) and ΔK_{model} is shown for two different occultations for the tangent height with the maximum aerosol signal. The residuals are displayed in the lower panel showing the accuracy of the fit.

[16] Unfortunately, it appears that the χ^2-value is flat for a wide range of size distributions. A modeled extinction for a small radius r_g and a large σ has a similar shape to that of a large radius r_g and a small σ. Therefore, both parameters of the aerosol size distribution cannot be determined at the same time, and an estimated σ-value is needed to get a best fit radius [*Steele et al.*, 2003, 2006].

[17] The retrieved *SC* was inverted into an actual vertical profile of aerosol loading by assuming a homogeneous cloud with 1 km layers using the same global fit method used for ACE retrievals *Boone et al.* [2005]. This assumption is not always realistic because the horizontal extent of the cloud is unknown. The location of the cloud along the slant path is

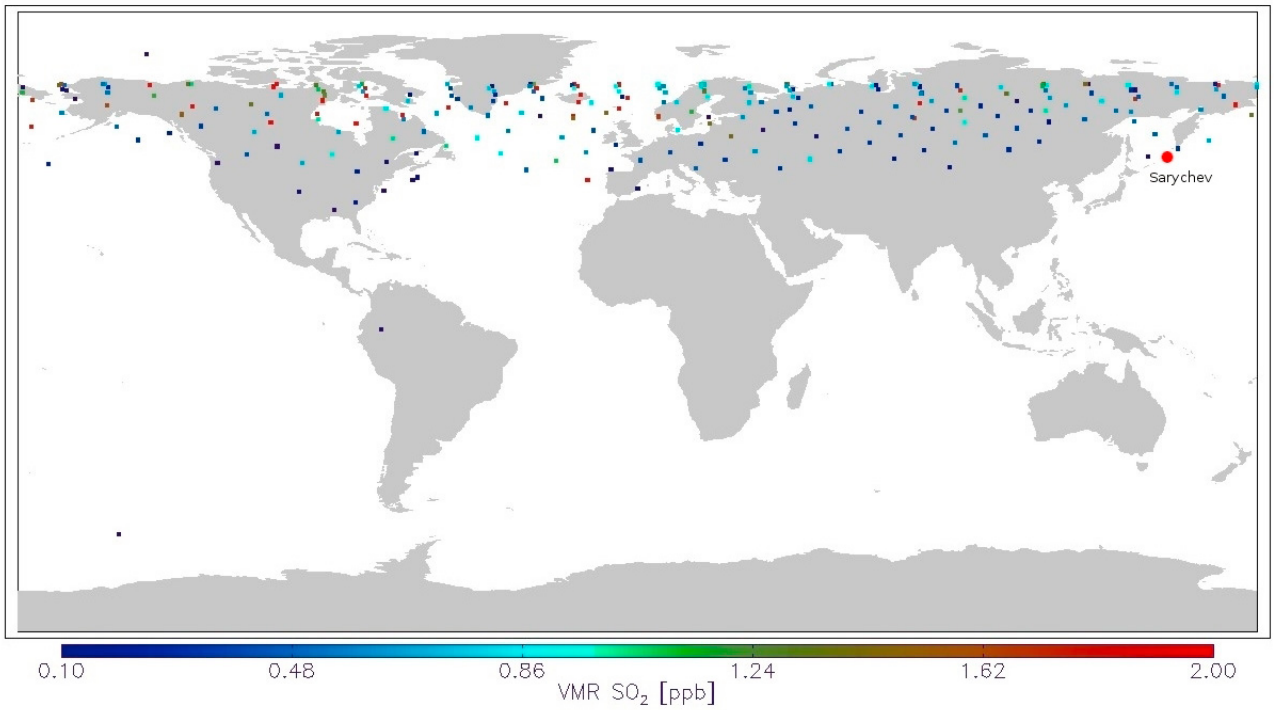

Figure 5. Map of occultation locations for July to September 2009 with an SO_2 VMR greater than 0.1 ppb (N = 247). The color indicates the maximum VMR for each occultation. The large red dot indicates the location of the Sarychev volcano.

not known so the retrieved tangent height represents a lower limit for the cloud height.

4. Data Analysis

4.1. Volcanic Plume Detection Following the Sarychev Eruption

[18] The first evidence of enhanced SO_2 from the eruption of the Sarychev volcano in ACE profiles occurred in July 2009, almost a month after the eruption, because the satellite's orbit precludes measurements during the latter part of June. As Figure 3 shows, a sulfur dioxide VMR greater than 0.1 ppb was detected in and just after July 2009, which reliably indicates the presence of a volcanic plume. Figure 5 shows the location of the 247 occultations (235 were observed in July 2009), in which a high SO_2 concentration was detected between July and September 2009. During the same months for 2007 and 2010 no occultations had SO_2 concentrations >0.1 ppb (in 2008 more than 250 occultations showed a enhanced SO_2 concentration due to the eruption of Kasatochi in August 2008). The volcanic plume spread over almost the entire Northern Hemisphere in the month just after the eruption, while the Southern Hemisphere is unaffected by the Sarychev volcano due to the long transportation time between the Hemispheres. Two occultations were found in the Southern Hemisphere (see Figure 5) with SO_2 VMRs of about 0.1 ppb, but this must be related to other volcanic activity in the Southern Hemisphere (e.g., Chaiten (Chile) or Ubinas (Peru) (AURA Cloud/Aerosol/SO_2 Working Group, online data, 2009)).

4.2. Observed Properties of the Aerosol Layer

[19] A strong aerosol layer can be seen in July 2009 in the ACE data in the Northern Hemisphere. Figure 6 shows the median atmospheric extinction (NIR-imager) averaged for different altitudes in steps of 1 km in July between 2004 and 2009 (there are currently no atmospheric extinction results available in the data set for July 2007), similar to that of *Sioris et al.* [2010]. In July 2009, the aerosol layer spans approximately 8.5 km to 17.5 km with a maximum extinction value of 0.0028 km^{-1} at an altitude of 13 km. Only in July 2009 can such an enhancement be seen and the usual atmospheric extinction at this altitude is about 0.0004 km^{-1}, almost one order of magnitude smaller. Figure 7a illustrates the profile of the SO_2 VMR (from ACE-FTS), the atmospheric extinction (from NIR-Imager) and the aerosol loading (derived from the ACE-FTS spectrum) from 14 July 2009 (68.31°N, 18.86°W), showing clear evidence of a layer in the lower stratosphere and a possible second peak at about 11.5 km. These three profiles are in good agreement with the plume height at approximately 15 km in all three cases. The atmospheric extinction has a maximum almost an order of magnitude greater than the average monthly median, while the SO_2 VMR reaches 5 ppb, the aerosol volume SC is 900 μm^3 cm^{-3} km and for a homogeneous cloud a volume density of almost 3 μm^3 cm^{-3} is achieved.

[20] Figure 7b shows another example for an occultation on 21 July 2009 (63.51°N, 176.37°W), showing clear evidence of a layer also at an altitude of 15 km. The profile of the aerosol loading does not show the same shape as the SO_2 VMR and atmospheric extinction. The reason could be the

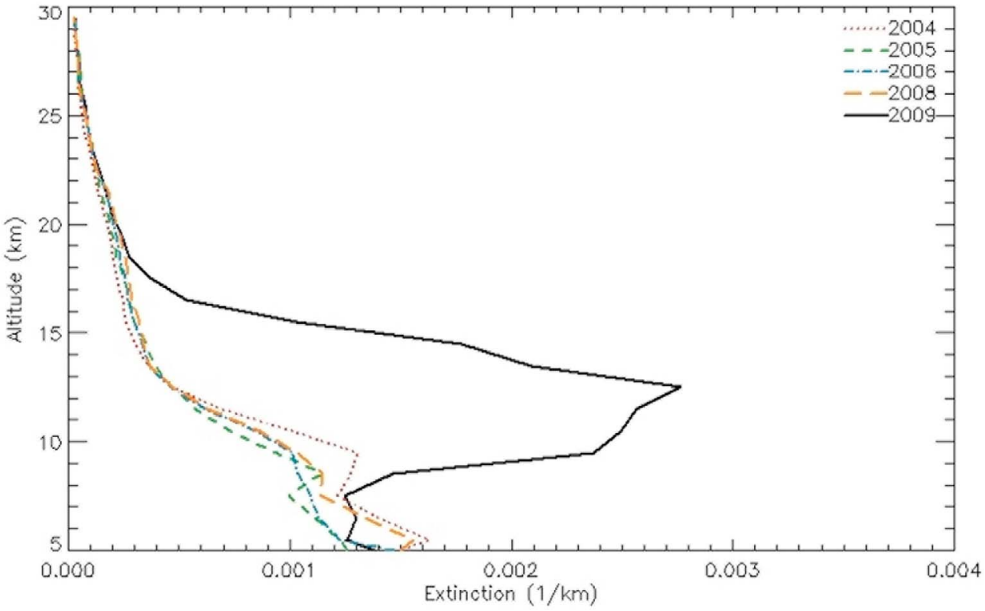

Figure 6. Median atmospheric extinction (NIR, v.2.2) in July from 2004 to 2009 in the Northern Hemisphere. An enhanced layer can be seen in July 2009 between 8.5 km and 17.5 km. July 2007 is excluded because the retrievals for this month are currently not available.

erroneous assumption of a homogeneous cloud layer for the retrieval of the aerosol loading from the *SC*, the unknown path length and the second lower plume layer below 10.5 km. The signal of volcanic aerosol is less than in the previous occultation, probably due to dilution of the plume, showing a maximum SO_2 VMR of almost 2 ppb at 15 km, the maximum atmospheric extinction of 0.01 km^{-1} and an aerosol loading of 1.5 μm^3 cm^{-3} at approximately 15 km. In Figure 8a profiles of the atmospheric extinction (NIR) between 5 and 30 km for the Northern Hemisphere are illustrated for July 2009 with a resolution of 5° in latitude. This layer of enhanced atmospheric extinction shows an aerosol layer between 9.5 km and 17.5 km for latitudes between 45°N and 70°N. A large enhancement of the extinction can be seen above the tropopause, which is shown by the black line. A similar shape can be seen in Figure 8b, which shows the median SO_2 VMR in the Northern Hemisphere in July 2009. A well-defined SO_2 layer is found between 12.5 km and 16.5 km from 45°N to 70°N. Figures 8a and 8b show the consistent pattern of SO_2 and enhanced atmospheric extinction from the Sarychev volcanic plume.

4.3. Observation of the Temporal Variation

[21] As shown in Figure 3 the SO_2 concentration cannot be reliably measured two months after the Sarychev eruption. The temporal variation of the SO_2 concentration cannot be monitored because the time period (one month) is too short due to the low spatial resolution and the small number of occultations. However, the temporal variation of the enhancement in atmospheric extinction can be observed with NIR-Imager data from ACE.

[22] Figure 9 shows the temporal evolution of the median atmospheric extinction (NIR) in the Northern Hemisphere. Figure 9 (bottom) shows the location (latitude) of the occultations used, while the sunset observations are indicated in red and sunrise in black. Notice that for August 2009 the occultations are between 0°N and 40°N, which results in a median tropopause at an altitude of 16 km. ACE is measuring close to the equator in August 2009 and the time for the plume to reach these tropical latitudes is relatively long. This explains why the Sarychev volcanic plume was not detected by ACE in August 2009 and the observed measurements correspond to the background extinction. Starting in July 2009 a clear enhancement layer can be seen and this layer persists until February 2010, when normal background conditions are reached again. This enhanced layer can be seen in the upper troposphere and lower stratosphere (the black line symbolizes the median tropopause of each month) between 50°N–70°N and descends approximately 1 km per month, while the mid-troposphere shows normal conditions throughout this time period.

[23] This evolution can also be confirmed by the average optical depth between 5.5 km and 25.5 km in altitude, shown in Figure 10. The optical depth in this altitude range has a background value of approximately 0.015. The optical depth in July and September is almost twice the normal value, starts decreasing in November 2009 and reaches pre-Sarychev conditions in February 2010. The reason for the increase in September and October 2009 could be the coagulation of the volcanic aerosols, which would lead to a greater optical density.

4.4. Size Distribution of the Sarychev Volcanic Aerosol

[24] The distribution width σ of Pinatubo and El Chichón volcanic aerosols were analyzed by *Deshler et al.* [1993] and *Hofmann and Rosen* [1983]. They obtained σ values between 1.6 and 2.0 after the first month of a volcanic eruption. Assuming that the Sarychev volcanic aerosol has similar properties, the σ value was fixed to 1.8 for our retrievals, while the parameters r_g, *SC* and *W* were derived

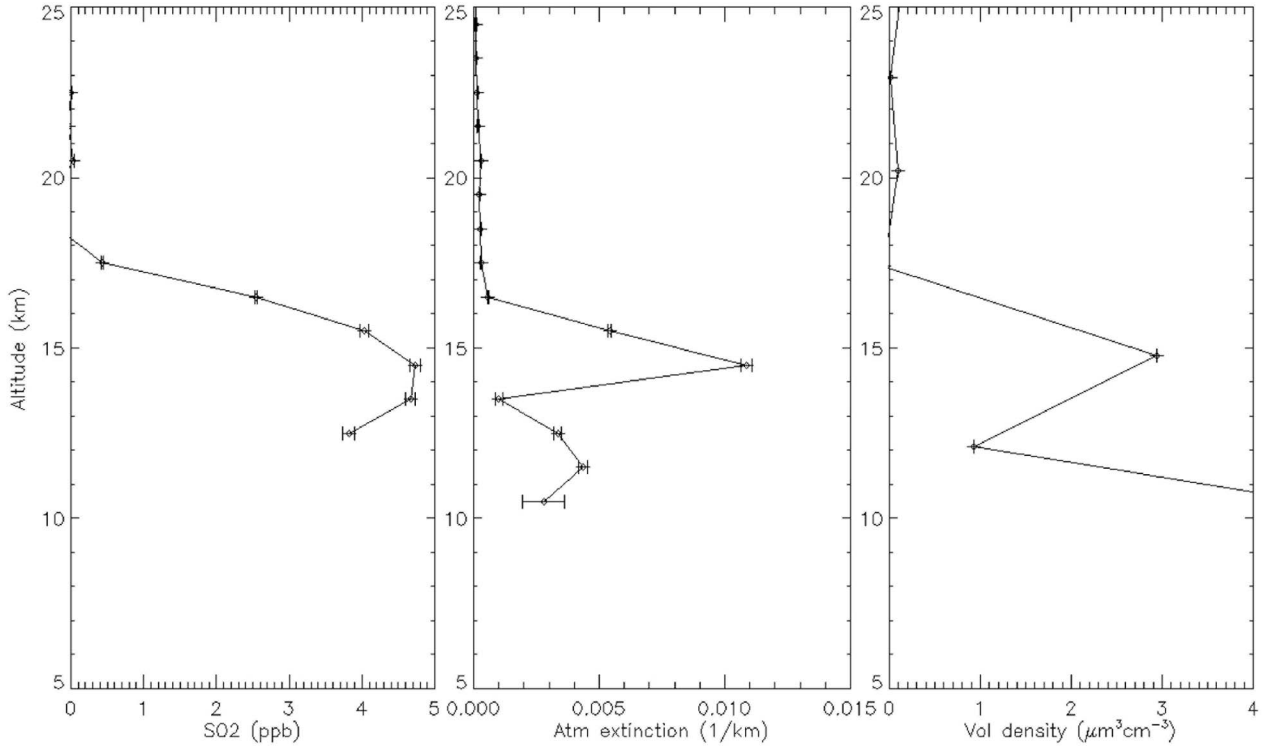

(a) ss31868 (14.07.2009, 68.31°N, 18.86°W)

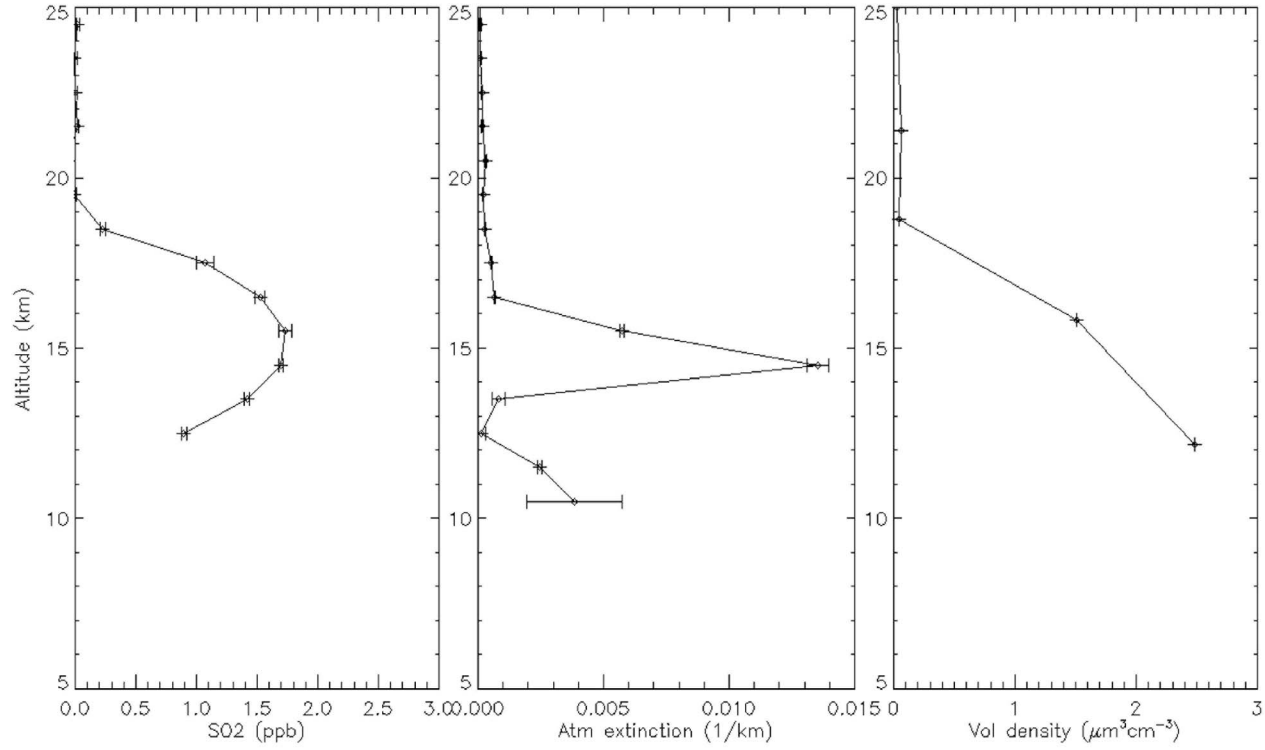

(b) ss31976 (21.07.2009, 63.51°N, 176.37°W)

Figure 7. The SO_2 VMR (ACE-FTS) profile, atmospheric extinction (NIR, v.2.2) and the aerosol loading (derived from ACE-FTS spectrum) is illustrated for two different occultations: (a) ss31868 (14 July 2009, 68.31°N, 18.86°W) and (b) ss31796 (21 July 2009, 63.51°N, 176.37°W). Note that the SO_2 and atmospheric extinction are on a 1 km altitude grid, but the aerosol retrieval is carried out for the spectra at the observed tangent height.

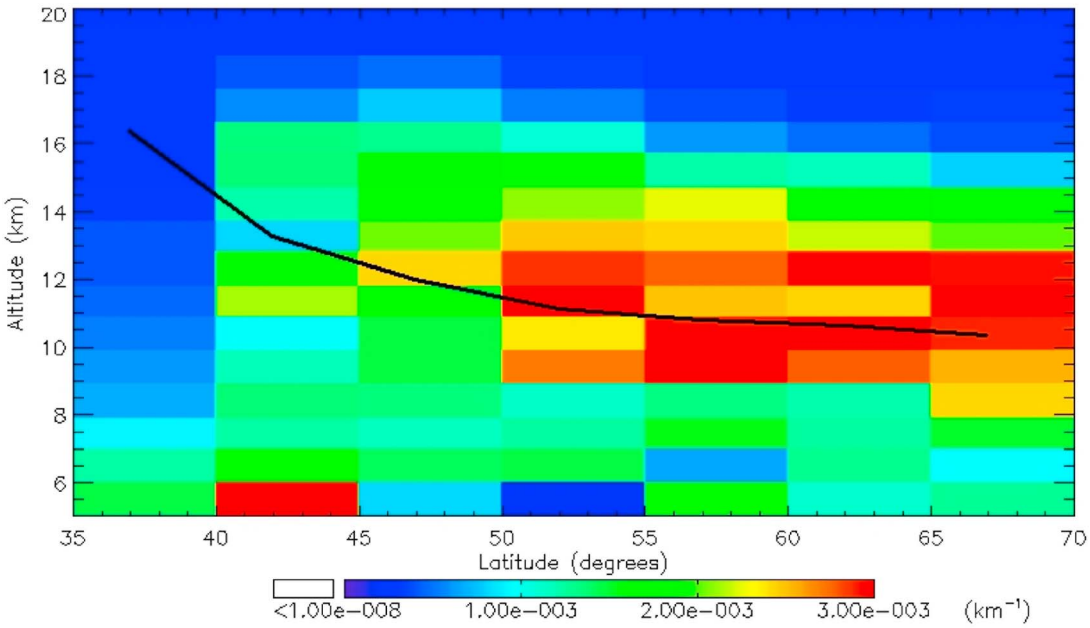

(a) Median atmospheric extinction (km^{-1}) (NIR, v.2.2) in July 2009.

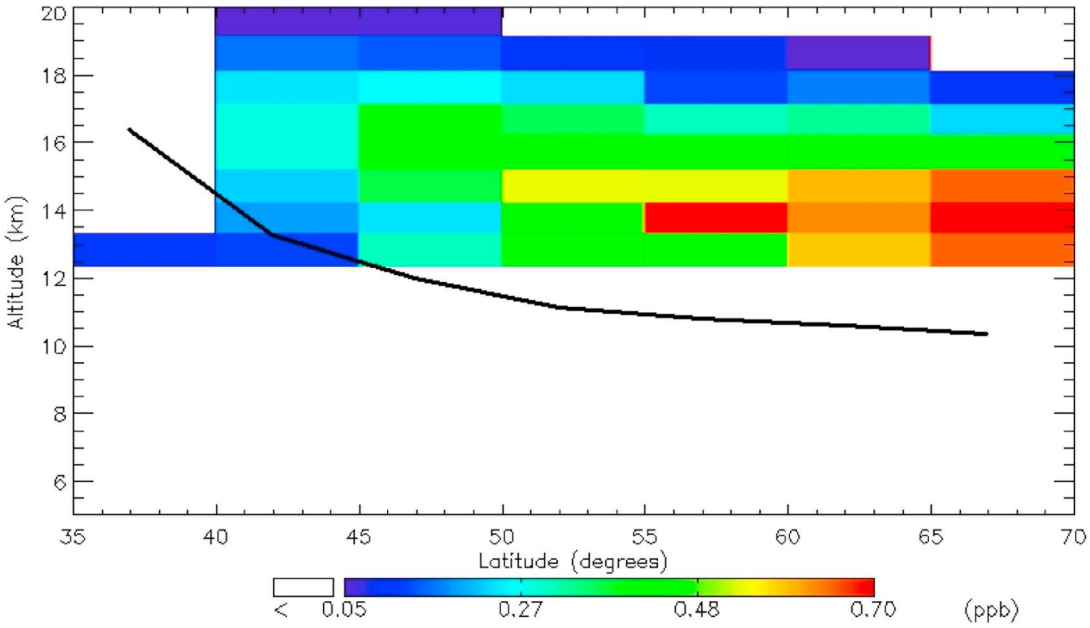

(b) Median SO_2 concentration (ppb) in July 2009.

Figure 8. Profile of the median (a) atmospheric extinction and (b) SO_2 VMR for July 2009 in the Northern Hemisphere. Both profiles show a clear layer between 45°N and 70°N. The black line is the median tropopause.

by least squares fitting. For the range of σ between 1.6 and 2.0, the radius r_g is in the range 0.052 μm $\leq r_g \leq$ 0.13 μm (ss31868) and 0.056 μm $\leq r_g \leq$ 0.14 μm (ss31976) at about 15 km (the lowest σ corresponds to the largest r_g). Figure 4 illustrates that the modeled aerosol spectra (for the mean distribution width σ = 1.8) reproduces the observed spectra well and results in a $\chi^2 \approx 2.5$ (Figure 4a, ss31868) and $\chi^2 \approx$ 1.4 (Figure 4b, ss31976). These two observations yield the same radius $r_g \approx 0.09$ μm for an approximately one month old Sarychev volcanic aerosol at about 15 km. The profile of the radius r_g, *SC* and *W* for the occultations ss31868 and ss31976 are presented in Figure 11. The *SC* and, therefore, the aerosol loading is smaller in occultation ss31976, which was taken one week after the ss31868 occultation, probably

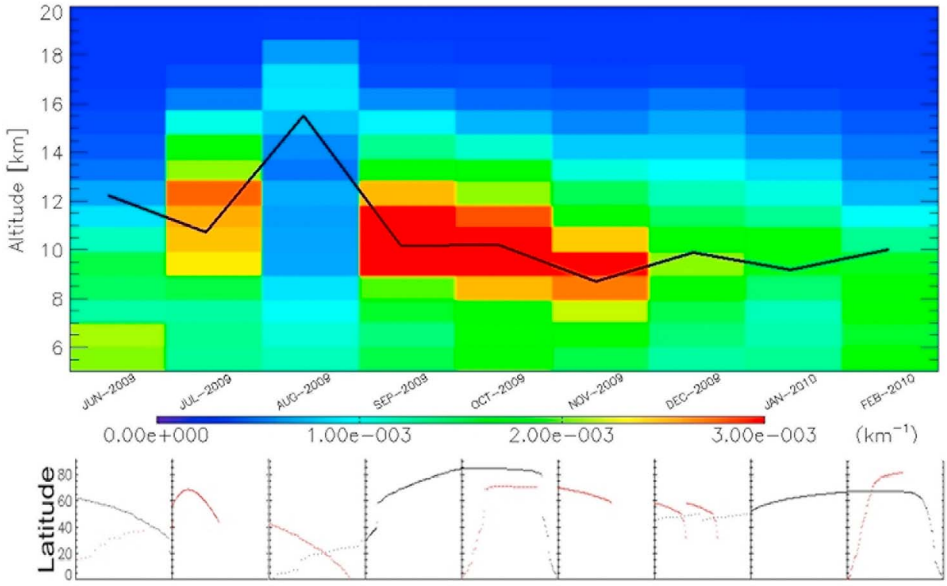

Figure 9. (top) Time series of the monthly median atmospheric extinction (km^{-1}) (NIR, v.2.2) between June 2009 and February 2010 in the Northern Hemisphere. The median tropopause is shown as a black line. (bottom) The location (latitude) of the measurements, where the black dots are the occultations observed at sunrise and the red dots those at sunset.

due to dilution of the volcanic plume. Note that this is not necessarily only a consequence of the measurements being a week apart. There is also the geographical difference to consider. The longitudes are very different (almost on opposite sides of the planet), and the latitudes differ by about 5°. As the altitude decreases the *SC* starts increasing at an altitude of 17 km (ss31868) and 18.5 km (ss31976), respectively. For the plume height (∼15 km) a composition of $W = 74.83 \pm 0.03\%$ (ss31868) and $W = 75.33 \pm 0.06\%$ (ss31976) sulfuric acid-water solution is retrieved and the radius has $r_g = 0.087 \pm 0.014$ μm and $r_g = 0.092 \pm 0.025$ μm, respectively. The *SC* at this altitude reaches $SC = 879.23 \pm 2.48$ μm^3 cm^{-3} km (ss31868) and $SC = 527.09 \pm 1.69$ μm^3 cm^{-3} km (ss31976), respectively. The statistical precision for *SC*, as well as for *W* with an error of less than 0.3% and 1.5%, respectively, is quite high. The surprisingly small error for SC probably is due to the very large number of channels at which the transmission is recorded. The precision of the retrieved radius is not as good, being between 15% and 30% relative to the retrieved value. For many altitudes the radius r_g cannot be derived because the aerosol signal is too low. It is only for heights with a relatively high

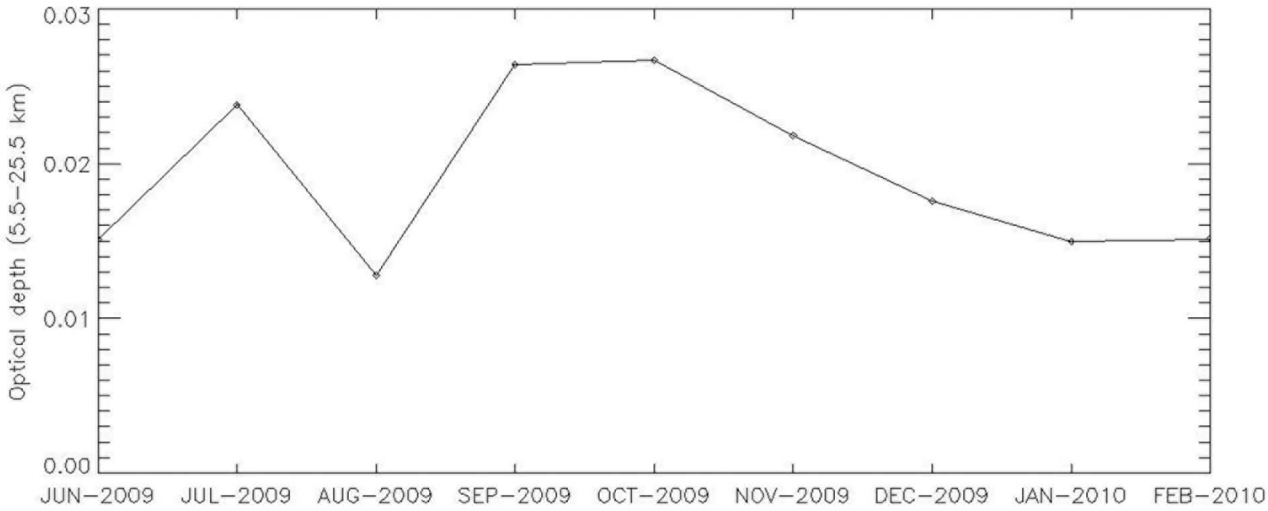

Figure 10. Monthly time series of the optical density (integrated median atmospheric extinction (NIR, v.2.2) between 5.5 km and 25.5 km) in the Northern Hemisphere between June 2009 and February 2010.

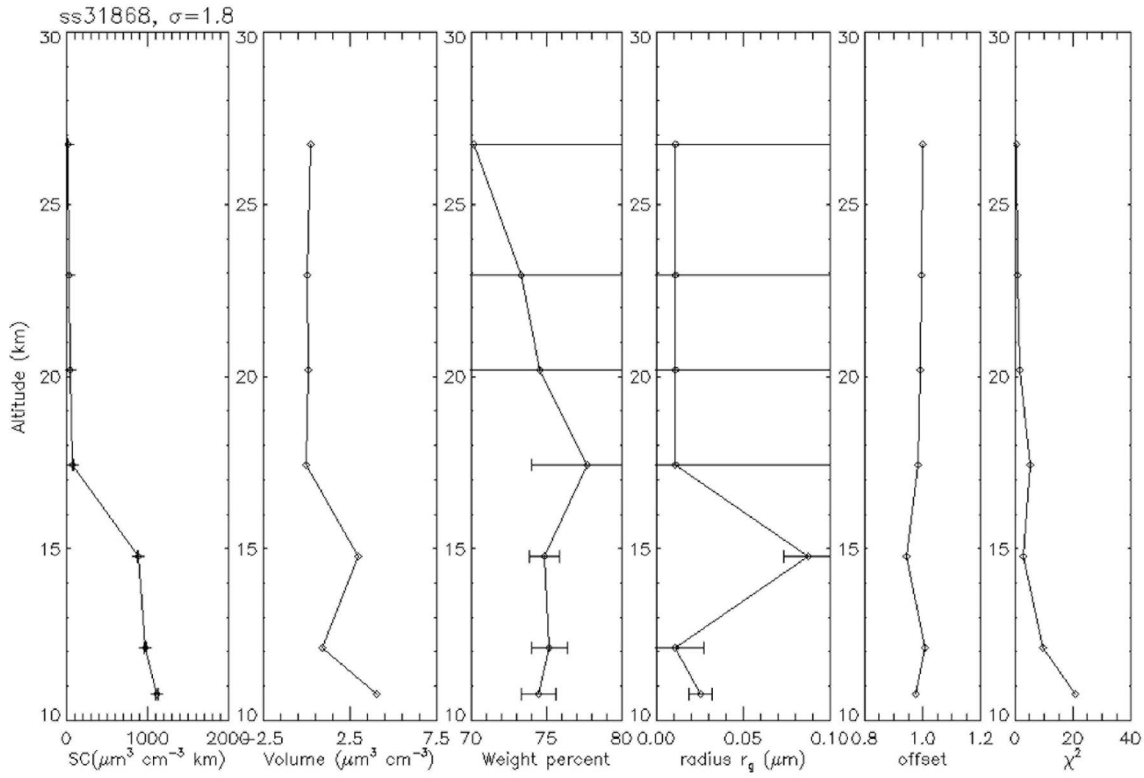

(a) ss31868 (14.07.2009, 68.31°N, 18.86°W)

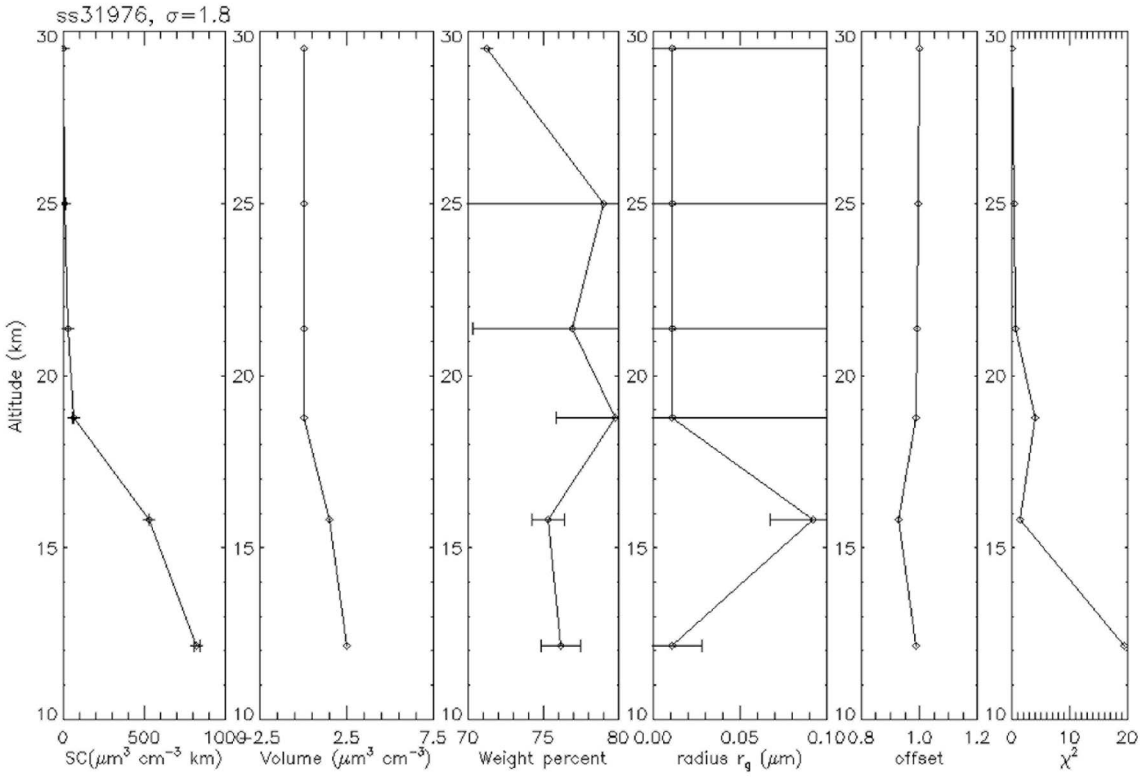

(b) ss31976 (21.07.2009, 63.51°N, 176.37°W)

Figure 11. Retrieved aerosol properties for two different occultations. Shown is the aerosol *SC*, the aerosol loading, *W*, r_g, the offset α and χ^2.

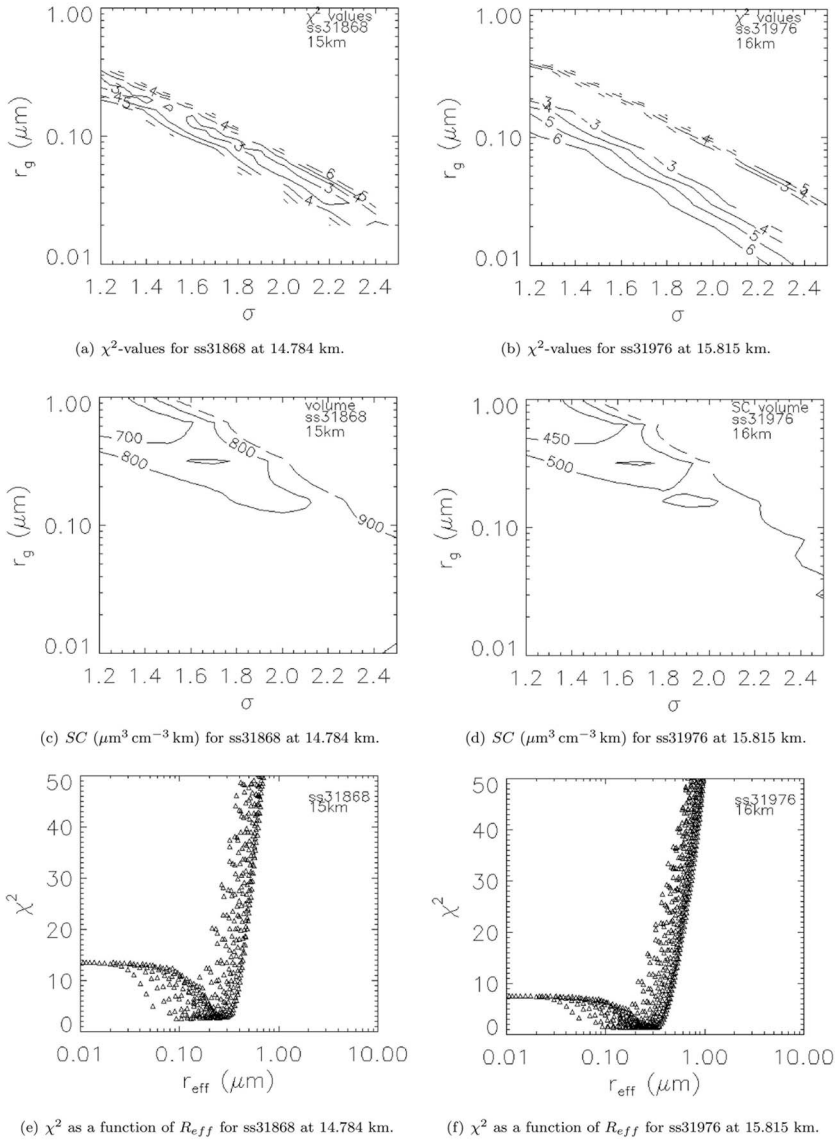

(a) χ^2-values for ss31868 at 14.784 km. (b) χ^2-values for ss31976 at 15.815 km.

(c) *SC* ($\mu m^3\,cm^{-3}$ km) for ss31868 at 14.784 km. (d) *SC* ($\mu m^3\,cm^{-3}$ km) for ss31976 at 15.815 km.

(e) χ^2 as a function of R_{eff} for ss31868 at 14.784 km. (f) χ^2 as a function of R_{eff} for ss31976 at 15.815 km.

Figure 12. Retrieved χ^2-values and *SC* as a function of r_g and σ, and χ^2 as a function of R_{eff} for two continuum spectra (a, c, e) ss31868 and (b, d, f) ss31976, at the height of the maximum aerosol signature.

aerosol loading that the radius can be derived with the least squares algorithm. This height almost always corresponds to the altitude with maximum aerosol extinction. In the case of a low aerosol concentration, the radius r_g is set to a value of r_g = 0.011 μm.

[25] However, as previously mentioned σ and r_g cannot be retrieved at the same time using only ACE infrared spectra and only under favorable circumstances can one of them be derived with our method, while the other aerosol size parameter is fixed. For the analysis presented in Figure 12, r_g and σ are fixed and *SC*, *W*, the offset α and χ^2 for the best fit are retrieved for a wide range of radii 0.01 μm $\leq r_g \leq$ 1.28 μm and distribution widths 1.2 $\leq \sigma \leq$ 2.5. In Figures 12a and 12b the χ^2-value is shown as a contour as a function of r_g and σ, showing that many different combinations of r_g and σ are possible. The minimum χ^2-values can be found in a wide diagonal band running from an r_g of almost 0.3 μm and a σ of 1.2 to an r_g of 0.02 μm with σ = 2.5. The change in *SC* and *W* for different combinations of r_g and σ inside the minimum χ^2-band is almost negligible, but given a value of sigma, r_g can be determined in the case of high aerosol loading. In the band of the minimum χ^2-values the *SC* corresponds to approximately 850 μm^3 cm^{-3} km (ss31868, Figure 12c) and 500 μm^3 cm^{-3} km (ss31976, Figure 12d), with a composition of 75% H_2SO_4 and 25% H_2O. These values give an aerosol loading between almost 3 μm^3 cm^{-3} (ss31868) and 1.5 μm^3 cm^{-3} (ss31796), while the background concentration for a similar time and location was found to be 0.13 μm^3 cm^{-3} at 15 km (typical background volume densities are between 0.2 and 0.3 μm^3 cm^{-3} at 15 km [*Steele et al.*, 1999]), which is an order of magnitude smaller than the observed aerosol loading one month after the Sarychev eruption.

[26] Our retrievals can be used to derive the effective radius R_{eff} (which is the ratio of the third moment of the size distribution to the second), as defined by *Hansen and Travis* [1974] for a single mode lognormal size distribution:

$$R_{eff} = r_g \cdot \exp\left(\frac{5}{2} \cdot \ln^2(\sigma)\right). \quad (12)$$

Steele et al. [2003] find that R_{eff} is a more useful variable than r_g to describe the aerosol size distribution. R_{eff} is shown in Figures 12e and 12f, and plotted against χ^2, showing the minimum χ^2-values result in an R_{eff} between 0.1 and 0.3 μm in both measurements. The effective radius has been analyzed for many other volcanic aerosols and leads to a value of R_{eff} of 0.1–0.2 μm for the Kasatochi and Pinatubo volcanoes almost one month after the eruption [*Mattis et al.*, 2010; *Ansmann et al.*, 1997]. This is in good agreement with our derived R_{eff} for the Sarychev aerosol one month after the eruption for the height of the maximum aerosol loading.

[27] The long term behavior of R_{eff} of volcanic aerosol (e.g., for Pinatubo [*Massie et al.*, 1996; *Ansmann et al.*, 1997; *Pueschel et al.*, 1994] and El Chichón [*Hofmann and Rosen*, 1983]) shows that the effective radius starts increasing with time directly after the volcanic eruption and a second radius mode, $r_{g,2} \approx 1$ μm [*Hofmann and Rosen*, 1983; *Deshler et al.*, 1993] appears approximately two months after the eruption due to coagulation of the aerosol particles. The very small particles ($r_g \leq 0.05$ μm) dilute or disperse after a few months as a result of the accretion on other particles [*Hofmann and Rosen*, 1983]. Approximately six months after the Pinatubo eruption the effective radius started to decrease slowly [*Ansmann et al.*, 1997].

[28] The radius retrieval method presented in this paper works only when the slant column is greater than a threshold value, $SC \geq 500$ μm^3 cm^{-3} km. The evolution of the aerosol size distribution cannot be seen in our measurements due to the lack of occultations with a high aerosol loading from aged volcanic plumes over a long period. The threshold aerosol loading was only reached in the month after the volcanic eruption of Sarychev. The only evidence of the increase in the particle size can be seen in the increase of the optical density (Figure 10) until October 2009 (four months after the eruption). After this time the optical density starts to decrease until in February 2010 normal pre-Sarychev conditions are reached again.

5. Conclusions

[29] For the first time SO_2 VMR profiles have been analyzed and sulfate aerosol properties have been determined using infrared data from the ACE mission. The work shows the observation and evolution of the Sarychev volcanic plume starting in July 2009. Plumes can be identified by both enhanced concentrations of SO_2 and the presence of sulfate aerosol bands in the observed infrared spectra. A volcanic plume in July 2009 has been found between 8.5 km and 17.5 km altitude using enhanced atmospheric extinction data from the ACE-Imager and enhanced SO_2 concentrations. The plume height declines by approximately 1 km per month based on near infrared imager profiles. One month after the eruption, the Sarychev volcanic plume spread over mid and high-latitudes of the Northern Hemisphere (between 55°N and 70°N), but did not reach the tropics. A similar spreading has been detected by IASI [*Haywood et al.*, 2010], where the highest SO_2 concentrations are between 55°N and 80°N and small perturbation reaches down to 35°N; however ACE does not have the same global coverage. No evidence of the presence of the Sarychev volcanic plume was observed after February 2010. The different analysis methods presented here: atmospheric extinction with the ACE-Imager, SO_2 VMRs retrieved from the ACE-FTS and aerosol loading determined by a least squares fitting of a modeled H_2SO_4 spectrum, show similar profiles and result in the same height of the plume.

[30] It has been shown that aerosol properties can be studied with the wide spectral coverage (820–4100 cm^{-1}) and high signal-to-noise ratio of ACE-FTS spectra using the method of *Eldering et al.* [2001]. The minimum slant column density required for a retrieval of the effective radius R_{eff} and the median radius r_g is approximately $SC \geq 500$ μm^3 cm^{-3} km. In addition to the H_2SO_4 aerosol, the extinction of an ice cloud was fitted using the observed continuum spectra with refractive indices taken from *Clapp et al.* [1995] and a unimodal lognormal distribution ($r_g = 2.5$ μm and $\sigma = 1.8$) [*Yang et al.*, 1997]. However, the spectral signature of this representative ice cloud is not present in the observed spectra. Cirrus clouds formed in association with a volcanic plume as it rises in the troposphere, are not present in the observed ACE spectra.

[31] In the two occultations presented in this paper, the maximum volume SC was 850 μm^3 cm^{-3} km (ss31868) and 500 μm^3 cm^{-3} km (ss31976), which results in an approximate aerosol loading of 3 μm^3 cm^{-3} (ss31868) and 1.5 μm^3 cm^{-3} (ss31796). The composition of the aerosol droplets was in both cases 75% H_2SO_4 and 25% H_2O. The calculation of these parameters is precise (but not necessarily accurate) and the derived statistical errors in SC and W are very small due to the large number of points over a wide spectral range available in the continuum spectra. The size distribution cannot be constrained uniquely but with a σ-value between 1.6 and 2.0 the radius r_g is in the range 0.052 μm $\leq r_g \leq$ 0.13 μm (ss31868) and 0.056 μm $\leq r_g \leq$ 0.14 μm (ss31976). The lowest χ^2-values (between 2.0 and 2.5) correspond to an R_{eff} of 0.1–0.3 μm. The retrieved offsets α equals one within error in most cases because the ACE-detectors are linear. Only at the peak height of the plume, where a high concentration of particles is present, is the offset α less than 1 (around 0.95), which indicates a reduced transmission. This may be caused by additional extinction of the solar radiation by ash particles in the volcanic plume.

[32] This paper serves to demonstrate the utility and information content of ACE infrared observations for the study of volcanic plumes. Sulfate aerosols from Kasatochi (Alaska, 2008), Merapi (Indonesia, 2010) and Grimsvötn (Iceland, 2011), and their evolution will be analyzed in the future using ACE data with the method demonstrated here. With the combination of ACE-FTS and MAESTRO spectra, the spectral range will be expanded and, therefore, the results improved. As shown by *Steele et al.* [2006], a wide spectral range that includes the visible region is very important in improving the precision of the retrieved parameters. The aerosol size distribution parameters are particularly sensitive

to the visible extinction and much lower aerosol loadings will be studied.

[33] **Acknowledgments.** The ACE mission is funded primarily by the Canadian Space Agency. Some funding was provided by the UK Natural Environment Research Council (NERC) through the National Centre for Earth Observation (NCEO). Work at the Jet Propulsion Laboratory, California Institute of Technology was carried out under contract with NASA.

References

Ansmann, A., I. Mattis, U. Wandinger, F. Wagner, J. Reichardt, and T. Deshler (1997), Evolution of the Pinatubo aerosol: Raman lidar observations of particle optical depth, effective radius, mass, and surface area over central Europe at 53.4°N, *J. Atmos. Sci.*, *54*, 2630–2641.

Bernath, P., et al. (2005), Atmospheric Chemistry Experiment (ACE): Mission overview, *Geophys. Res. Lett.*, *32*, L15S01, doi:10.1029/2005GL022386.

Boone, C., R. Nassar, K. A. Walker, Y. Rochon, S. D. McLeod, C. P. Rinsland, and P. F. Bernath (2005), Retrievals for the atmospheric chemistry experiment Fourier transform spectrometer, *Appl. Opt.*, *44*, 7218–7231.

Clapp, M. L., R. E. Miller, and D. R. Wornsnop (1995), Frequency-dependent optical constants of water ice obtained directly from aerosol extinction spectra, *J. Phys. Chem.*, *99*, 6317–6326.

Deshler, T., B. J. Johnson, and W. R. Rozier (1993), Balloonborne measurements of Pinatubo aerosol during 1991 and 1992 at 41°N: Vertical profiles, size distributions, and volatility, *Geophys. Res. Lett.*, *20*, 1435–1438.

Dufour, G., S. Szopa, M. P. Barkley, C. D. Boone, A. Perrin, P. I. Palmer, and P. F. Bernath (2009), Global upper-tropospheric formaldehyde: seasonal cycles observed by the ACE-FTS satellite instrument, *Atmos. Chem. Phys.*, *9*, 3893–3910.

Dutton, E. G., and J. R. Christy (1992), Solar radiative forcing at selected locations and evidence for global lower tropospheric cooling following the eruption of El Chichon and Pinatubo, *Geophys. Res. Lett.*, *19*, 2313–2316.

Eldering, A., F. W. Irion, A. Y. Chang, M. R. Gunson, F. P. Mills, and H. M. Steele (2001), Vertical profiles of aerosol volume from high-spectral-resolution infrared transmission measurements, I. Methodology, *Appl. Opt.*, *40*, 3082–3091.

Eldering, A., B. H. Kahn, F. P. Mills, F. W. Irion, H. M. Steele, and M. R. Gunson (2004), Vertical profiles of aerosol volume from high-spectral-resolution infrared transmission measurements: Results, *J. Geophys. Res.*, *109*, D20201, doi:10.1029/2004JD004623.

Foucher, P. Y., A. Chédin, R. Armante, C. Boone, C. Crevoisier, and P. Bernath (2011), Carbon dioxide atmospheric vertical profiles retrieved from space observation using ACE-FTS solar occultation instrument, *Atmos. Chem. Phys.*, *11*, 2455–2470.

Gilbert, K. L., D. N. Turnbull, K. A. Walker, C. D. Boone, S. D. McLeod, M. Butler, R. Skelton, P. F. Bernath, F. Chateauneuf, and M.-A. Soucy (2007), The onboard imagers for the Canadian ACE SCISAT-1 mission, *J. Geophys. Res.*, *112*, D12207, doi:10.1029/2006JD007714.

González Abad, G., et al. (2011), Ethane, ethyne and carbon monoxide concentrations in the upper troposphere and lower stratosphere from ACE and GEOS-Chem: A comparison study (2011), *Atmos. Chem. Phys. Discuss.*, *11*, 13,099–13,139.

Gunson, M. R., et al. (1996), The Atmospheric Trace Gas Spectroscopy (ATMOS) experiment: Deployment on the ATLAS Space Shuttle mission, *Geophys. Res. Lett.*, *23*, 2333–2339.

Hansen, J. E., and L. D. Travis (1974), Light scattering in planetary atmospheres, *Space. Sci. Rev.*, *16*, 527–610.

Haywood, J. M., et al. (2010), Observation of the eruption of the Sarychev volcano and simulations using the HadGEM2 climate model, *J. Geophys. Res.*, *115*, D21212, doi:10.1029/2010JD014447.

Hofmann, D. J., and J. M. Rosen (1983), Sulfuric acid droplet formation and growth in the stratosphere after the 1982 eruption of El Chichon, *Science*, *222*, 325–327.

Massie, S. T., T. Deshler, G. E. Thomas, J. L. Mergenthaler, and J. M. Russell (1996), Evolution of the infrared properties of the Mount Pinatubo aerosol cloud over Laramie, Wyoming, *J. Geophys. Res.*, *101*, 23,007–23,019.

Mattis, I., P. Siefert, D. Müller, M. Tesche, A. Hiebsch, T. Kanitz, J. Schmidt, F. Finger, U. Wandinger, and A. Ansmann (2010), Volcanic aerosol layers observed with multiwavelength Raman lidar over central Europe in 2008–2009, *J. Geophys. Res.*, *115*, D00L04, doi:10.1029/2009JD013472.

McElroy, C. T., et al. (2007), The ACE-MAESTRO instrument on SCISAT: Description, performance, and preliminary results, *Appl. Opt.*, *46*, 4341–4356.

McHugh, M., B. Magill, K. A. Walker, C. D. Boone, P. F. Bernath, and J. M. Russell (2005), Comparison of atmospheric retrievals from ACE and HALOE, *Geophys. Res. Lett.*, *32*, L15S10, doi:10.1029/2005GL022403.

Pinnick, R. G., J. M. Rosen, and D. J. Hofmann (1976), Stratospheric aerosol measurements: III. Optical model calculations, *J. Atmos. Sci.*, *33*, 304–314.

Pollack, J. B., O. B. Toon, C. Sagan, A. Summers, B. Baldwin, and W. van Camp (1976), Volcanic explosion and climatic change: A theoretical assessment, *J. Geophys. Res.*, *81*, 1071–1083, doi:10.1029/JC081i006p01071.

Pueschel, R. F., P. B. Russell, D. A. Allen, G. V. Ferry, K. G. Snetsinger, J. M. Livingston, and S. Verma (1994), Physical and optical properties of the Pinatubo volcanic aerosol: Aircraft observations with impactors and a Sun-tracking photometer, *J. Geophys. Res.*, *99*, 12,915–12,922.

Reeves, C. E., and S. A. Penkett (2003), Measurements of peroxides and what they tell us, *Chem. Rev.*, *103*, 5199–5218.

Reiner, T., and F. Arnold (1994), Laboratory investigation of gaseous sulfuric acid formation via $SO_3+H_2O+M \rightarrow H_2SO_4+M$: Measurement of the rate constant and product identification, *J. Chem. Phys.*, *101*, 7399–7407.

Rothman, L. S., et al. (2005), The HITRAN 2004 molecular spectroscopic database, *J. Quant. Spectrosc. Radiat. Transfer*, *96*, 139–204.

Sato, M., J. E. Hansen, M. P. McCormick, and J. B. Pollack (1993), Stratospheric Aerosol optical depths, 1850–1990, *J. Geophys. Res.*, *98*, 22,987–22,994.

Sheridan, P. J., R. C. Schnell, D. J. Hofmann, and T. Deshler (1992), Electron microscope studies of Mt. Pinatubo aerosol layers over Laramie, Wyoming during summer 1991, *Geophys. Res. Lett.*, *19*, 203–206.

Sica, M. L., et al. (2008), Validation of the Atmospheric Chemistry Experiment (ACE) version 2.2 temperature using ground-based and space-borne measurements, *Atmos. Chem. Phys.*, *8*, 35–62.

Sioris, C. E., C. D. Boone, P. F. Bernath, J. Zou, C. T. McElroy, and C. A. McLinden (2010), Atmospheric Chemistry Experiment (ACE) observations of aerosol in the upper troposphere and lower stratosphere from the Kasatochi volcanic eruption, *J. Geophys. Res.*, *115*, D00L14, doi:10.1029/2009JD013469.

Steele, H. M., J. D. Lumpe, R. P. Turco, R. M. Bevilacqua, and S. T. Massie (1999), Retrievals of aerosol surface area and volume densities from extinction measurements: Application to POAM II and SAGE II, *J. Geophys. Res.*, *104*, 9325–9336.

Steele, H. M., A. Eldering, B. Sen, G. C. Toon, F. P. Mills, and B. H. Kahn (2003), Retrieval of stratospheric aerosol size and composition information from solar infrared transmission spectra, *Appl. Opt.*, *43*, 2140–2154.

Steele, H. M., A. Eldering, and J. D. Lumpe (2006), Simulations of the accuracy in retrieving stratospheric aerosol effective radius, composition, and loading from infrared spectral transmission measurements, *Appl. Opt.*, *45*, 2014–2027.

Tisdale, R. T., D. L. Glandorf, M. A. Tolbert, and O. B. Toon (1998), Infrared optical constant of low-temperature H_2SO_4 solutions representative of stratospheric sulfate aerosol, *J. Geophys. Res.*, *103*, 25,353–25,370.

Vanhellemont, F., et al. (2008), Aerosol extinction profiles at 525 nm and 1030 nm derived from ACE imager data: Comparisons with GOMOS, SAGE II, SAGE III, POAM III, and OSIRIS, *Atmos. Chem. Phys.*, *8*, 2027–2037.

Yang, P., K. N. Liou, and W. P. Arnott (1997), Extinction efficiency and single-scattering albedo for laboratory and natural cirrus clouds, *J. Geophys. Res.*, *102*, 21,825–21,835, doi:10.1029/97JD01768.

C. D. Boone, Department of Chemistry, University of Waterloo, 200 University Ave. W, University of Waterloo, Waterloo, ON N2L 3G1, Canada.

D. Doeringer, Department of Physics, University of York, York YO10 5DD, UK. (dd557@york.ac.uk)

A. Eldering, Jet Propulsion Laboratory, MS 183-601, 4800 Oak Grove Dr., Pasadena, CA 91109-8099, USA.

G. González Abad and P. F. Bernath, Department of Chemistry, University of York, York YO10 5DD, UK.